New insight into the ZnO sulfidation reaction: mechanism and kinetics modeling of the ZnS outward growth

Laure Neveux, David Chiche, Javier Perez-Pellitero, Loïc Favergeon, Anne-Sophie Gay, Michèle Pijolat

New insight into the ZnO sulfidation reaction:mechanism and kinetics modeling of the ZnS outward growth

Laure Neveux[ab] ; David Chiche[a] ; Javier Perez-Pellitero[a] ; Loïc Favergeon[b] ; Anne-Sophie Gay[a] ; Michèle Pijolat[b]

a IFP Energies nouvelles, Rond-point de l'échangeur de Solaize, BP 3, 69360 Solaize, France. E-mail: david.chiche@ifpen.fr

b Ecole Nationale Supérieure des Mines, SPIN-EMSE, Département Pressic, LGF, F-42023 Saint-Etienne, France. E-mail: mpijolat@emse.fr

Abstract

Zinc oxide based materials are commonly used for the final desulfurization of synthesis gas in Fischer–Tropsch based XTL processes. Although the ZnO sulfidation reaction has been widely studied, little is known about the transformation at the crystal scale, its detailed mechanism and kinetics. A model ZnO material with well-determined characteristics (particle size and shape) has been synthesized to perform this study. Characterizations of sulfided samples (using XRD, TEM and electron diffraction) have shown the formation of oriented polycrystalline ZnS nanoparticles with a predominant hexagonal form (wurtzite phase). TEM observations also have evidenced an outward development of the ZnS phase, showing zinc and oxygen diffusion from the ZnO–ZnS internal interface to the surface of the ZnS particle. The kinetics of ZnO sulfidation by H_2S has been investigated using isothermal and isobaric thermogravimetry. Kinetic tests have been performed that show that nucleation of ZnS is instantaneous compared to the growth process. A reaction mechanism composed of eight elementary steps has been proposed to account for these results, and various possible rate laws have been determined upon approximation of the rate-determining step. Thermogravimetry experiments performed in a wide range of H_2S and H_2O partial pressures have shown that the ZnO sulfidation reaction rate has a nonlinear variation with H_2S partial pressure at the same time no significant influence of water vapor on reaction kinetics has been observed. From these observations, a mixed kinetics of external interface reaction with water desorption and oxygen diffusion has been determined to control the reaction kinetics and the proposed mechanism has been validated. However, the formation of voids at the ZnO–ZnS internal interface, characterized by TEM and electron tomography, strongly slows down the reaction rate. Therefore, the impact of the decreasing ZnO–ZnS internal interface on reaction kinetics has been taken into account in the reaction rate expression. In this way the void formation at the interface has been modeled considering a random nucleation followed by an isotropic growth of cavities. Very good agreement has been observed between both experimental and calculated rates after taking into account the decrease in the ZnO–ZnS internal interface.

1. Introduction

Among the second generation biofuels processes, the BTL process (for ''Biomass To Liquid'') aims at turning agricultural wastes into fuel. More generally, Fischer–Tropsch based XTL processes (X = Biomass, Coal, or Gas) comprise a first step of feed gasification into a synthesis gas or syngas composed of a CO–H_2 mixture. [1] After multiple gas conditioning steps aimed at reaching the required specifications,[2,3] the syngas undergoes the Fischer–Tropsch reaction in order to produce synthetic liquid fuel.[4,5] However, this reaction is catalyzed and the syngas must not contain any impurities, such as sulfur species, in order to avoid catalyst poisoning.[6,7] Deep desulfurization of synthesis gas is generally achieved with solids made up of metal oxides, such as zinc oxide, which can react with H_2S according to the reaction:

$$ZnO\ (s) + H_2S\ (g) \rightarrow ZnS\ (s) + H_2O\ (g)$$

Although the ZnO sulfidation reaction has been widely studied at a macroscopic scale and in the scope of industrial applications, little is known about the mechanism and reaction kinetics involved in the solid state transformation of zinc oxide crystals into zinc sulfide in the presence of H_2S, as also highlighted in a recent review of Samokhvalov and Tatarchuk.[8] The previously published kinetic studies have been achieved thanks to thermogravimetry experiments, but industrial shaped solids have been often used for this purpose.[9–12] Models based on the shrinking core model (grain model, pore model),[13] including porosity aspects, have been frequently used to represent gas–solid reactions and in particular the ZnO sulfidation reaction.[14,15] In these studies, the authors have followed the evolution of solid porosity and sintering during the sulfidation reaction. The results emerging from the models have been then compared to experimental data and good agreement has been observed. However, the models used to represent the reaction have supposed an inward growth of the zinc sulfide phase (namely a ''shrinking core'') assuming the diffusion of sulfur species in crystalline ZnO particles. This was indeed arbitrary as the whole reaction mechanism has not been described accurately, and no clear evidence of a mechanism involving sulfur diffusion has been proven. Indeed, very few studies have discussed the reaction mechanism, and no study has described the elementary steps involved in the reaction mechanism at a crystal scale. A small number of reports on real-time in situ experimental determination of the transformation at a crystal scale of the ZnO sulfidation reaction can be found.[8] Only one study has referred to the mechanism of the reaction of H_2S with the surface of ZnO by diffuse reflectance FTIR.[16] The conversion of H_2S into ZnS by successive proton transfers to chemisorbed hydroxyls on the Zn- and O-polar faces has been proposed, but no proposition for the bulk transformation mechanism was reported. Moreover, no rate-determining step for the ZnO sulfidation reaction has been clearly identified. For that purpose, some studies related to the influence on the kinetic rate of the partial pressures of the gases involved in the ZnO sulfidation are reported. Many studies have found that the reaction rate increases with H_2S concentration at constant temperature.[14,17–19] Besides, the reaction was found to be of first order with respect to H_2S concentration under isothermal conditions.[11,20] However, no clear dependence of the reaction rate towards H_2O partial pressure has been demonstrated. Indeed, according to one study, the presence of water vapor appears to interfere with the reaction between ZnO and H_2S and decreases the reaction kinetics.[21] Some other studies have found that the presence of water increases the reaction rate at the beginning of the reaction between ZnO and H_2S and that ZnO conversion is promoted by water vapor.[19,22–24] Another study has

shown no effect of water on the initial rate of the sulfidation reaction.[25] From these observations, it appears that water and H_2S influence on ZnO sulfidation kinetics has to be investigated and clarified.

In a previous work, various model ZnO materials with well-determined characteristics have been synthesized and characterized after sulfidation.[26] Characterizations of the reaction products using electronic microscopies have indicated that a polycrystalline ZnS layer is formed around the monocrystalline ZnO particles and cavities in the bulk of ZnO have been noticed at partial conversion. At total conversion, a void has been observed in the core of the sulfided particles, which has indicated that ZnS is more likely to be formed through an outward growth mechanism. This observation consequently implies for the sulfidation mechanism, a zinc and oxygen diffusion through the ZnS layer from the internal interface ZnO–ZnS to the surface of the ZnS particle and no sulfur diffusion. Therefore, regarding the ZnO sulfidation reaction, the relevance of the widely used shrinking core based models has to be reconsidered.

In this article, we provide additional evidences for outward growth mechanisms for the ZnO sulfidation reaction, based on transmission electron microscopy and electron tomography characterizations. This work also brings rational experimental kinetic data, performed through thermogravimetry experiments, in order to determine a reaction mechanism of the solid transformation, and to establish a kinetic rate model.

2. Experimental

2.1. ZnO synthesis

A ZnO material was synthesized by thermal decomposition of zinc acetate at 500°C ($Zn(CH_3COO)_2,2H_2O$ from Prolabo, purity >99.9%). Mono-crystalline ZnO rods with hexagonal sections were obtained, that exhibited a length of 500–1000 nm, a diameter of approximately 50 nm (*cf.* SEM micrographs shown in Fig. 3a.), and a specific surface area of 6 $m^2\ g^{-1}$.

2.2. Thermogravimetry

The sulfidation of ZnO was followed by thermogravimetry, in the temperature range from 200 to 400°C and at atmospheric pressure, using a commercial magnetic suspension balance (Rubotherm) with a flowing mixture (from 0.5 to 3.5 NL h^{-1}) of hydrogen sulfide (from 1.6 to 100 kPa H_2S partial pressure) diluted in helium or nitrogen. The balance was equipped with a three lines gas dosing system. One line was outfitted with a saturator in order to introduce water vapor into the gaseous phase. The sample weight (~10 mg) was sufficiently low to prevent any effect of gases pressure gradients in the powder layer. To perform measurements, the sample was heated to the desired temperature under a helium or nitrogen flow, then once the target temperature was reached, the gas mixture of hydrogen sulfide and helium or nitrogen was introduced into the balance under isobaric and isothermal conditions.

2.3. Material characterizations

X-ray powder diffraction patterns (XRD) were recorded using a PANalytical X'Pert PRO diffractometer operating with CuKα radiation (λ = 1.54182 Å). XRD patterns were measured over the 2θ interval 20–80°.

Scanning electron microscopy (SEM) observations were performed using a JEOL JSM-6340F (Field Emission Scanning Electron Microscope) apparatus operating at 1 kV. Transmission electron microscopy (TEM) observations and electron tomography were performed using a JEOL 2100F–FEG (Field Emission Gun) apparatus operating at 200 kV.

For electron tomography, the samples were suspended in ethanol and sonicated. A droplet of the suspension was deposited on a copper TEM grid coated by a holey carbon film. A droplet of a suspension of 5 nm gold nanoparticles was then applied on the grid. Images were taken in bright field mode by rotating the sample in the electron beam over an angular range of ±70° using a 1.5° tilt increment, in the Saxton scheme, which corresponds to 130 pictures. Alignment of the TEM tilt series was performed thanks to gold fiducial markers, 3D reconstruction was realized by filtered back projection.

Material specific surface areas were determined from nitrogen adsorption isotherms. N_2 adsorption–desorption isotherms were measured at 77 K using a Micromeritics ASAP 2420 apparatus. Specific surface areas were calculated using the BET (Brunauer–Emmet–Teller) relation.

3. Results and discussion

3.1. Heterogeneous kinetics approach

The following heterogeneous kinetics bases developed to study gas–solid reactions have been carried out. For gas–solid reactions, it is well admitted that two processes are involved in the development of the solid product: nucleation and growth.[27] Growth process can occur either with an outward or an inward development, and is composed of a succession of elementary steps. Each step occurs in a zone (external interface, diffusion layer or internal interface), and in the most simple case, one step kinetically controls the reaction rate (rate-determining step).

The assumption of a growth rate-determining step can be verified using the method of the sudden changes in temperature or pressure, as further explained in Section 3.4.[28] The measurements using the method of sudden changes rely on the use of eqn (1) for the rate of reaction:

$$\frac{d\alpha}{dt} = \phi(T, P_i) S_m(t) \quad (1)$$

with P_i the partial pressure of each gaseous compound i involved in the reaction. $\phi(T,P_i)$, called the areic reactivity of growth, expressed in mol m^{-2} s^{-1}, represents a kinetic constant, which depends on the operating conditions. $S_m(t)$, expressed in m^2 mol^{-1}, is related to the extent of the geometrical zone (surface, diffusion layer, internal interface), where the rate-determining step of growth occurs. These functions are more general than k and $f(\alpha)$ in the classical $d\alpha/dt = k\, f(\alpha)$ equation since ϕ is not constrained to vary with the temperature according to the Arrhenius law, and S_m is not

necessarily an analytical function of the fractional conversion and depends on the kinetic model (geometry of the initial particle, growth direction, location of the rate-determining step).

3.2. Kinetic measurements

The kinetic curves have been obtained through thermogravimetric experiments with a thin amount of powder in a crucible in order to ascertain isobaric and isothermal conditions in the reaction bed. Indeed, powders are adapted for kinetic studies since they allow us to have results independent of the shaping of solids, and to free oneself from the intragranular porosity that may affect reaction kinetics.

Kinetic curves obtained for the sulfidation of the ZnO sample are reported in Fig. 1. Fig. 1a shows the fractional conversion α as a function of time, deduced from thermogravimetry experiments performed at 310°C, 5 kPa H_2S partial pressure and 2.5 kPa H_2O partial pressure. The fractional conversion is defined as $\alpha = \Delta m(t)/\Delta m(total)$, where $\Delta m(t)$ represents the experimental gain of mass during sulfidation reaction, and $\Delta m(total)$ represents the theoretical mass increase expected for total conversion. The reaction rate $d\alpha/dt$ as a function of the fractional conversion a deduced from $\alpha(t)$ is reported in Fig 1b.

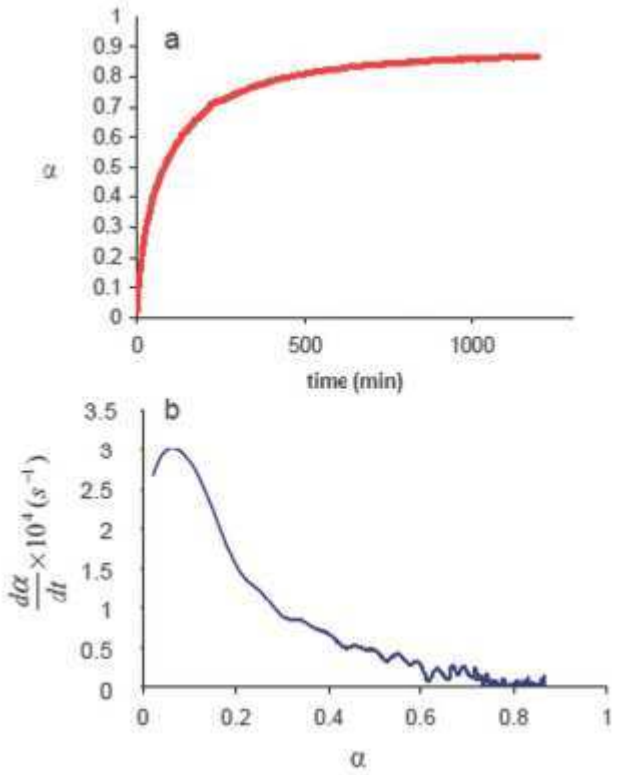

Figure 1 : (a) variation of the fractionnal conversion versus time of ZnO sulfidation at 310°C, P(H_2S)=5kPa and P(H_2O)=2,5kPa. (b) variation of the reaction rate $d\alpha/dt$ as a function of fractionnal conversion α.

The shape of the curves reveals a kinetic blocking ($d\alpha/dt \rightarrow 0$), which may restrain the reaction for a values above ~0.7. Indeed the final conversion never reached 100% even if the duration of the experiment was significantly increased.

The initial increase in dα/dt (from 0 up to a fractional conversion value around 0.1 (at t~10 min)) is due to the increasing H_2S partial pressure during the filling of the measuring cell. Thereby, at the very beginning of the reaction, the reaction is limited to the provision of H_2S, which gives to the rate curve this particular bell-shape. The experimental curve was consequently corrected in order to be able to compare experimental rates to those calculated for isobaric conditions. To perform that correction, the H_2S concentration profile versus time was expressed according to eqn (2):

$$F_p = \frac{P(H_2S)}{P(H_2S)_0} = \left(1 - e^{-t/\tau}\right) \quad \text{with } \tau = \frac{V}{Q} \qquad (2)$$

where V stands for the measuring cell volume (0.39 x 10^{-3} m^3), Q the gas flow rate (m^3 h^{-1}), t the time (h), $P(H_2S)_0$ is the H_2S partial pressure of the feed gas, $P(H_2S)$ is the H_2S partial pressure in contact with the sample at instant t. As the reaction rate seems to vary according to the law $v = kP(H_2S)^{0.55}$ (as further discussed in Section 3.6, cf. Fig. 13 and 14), the correction of the reaction rates can be performed using eqn (3):

$$v_{corr} = \frac{v_{exp}}{\left(F_p(\alpha)\right)^{0.55}} \qquad (3)$$

As shown in Fig. 2, the corrected experimental rate curve does not exhibit any more a bell-shape feature and can be compared to a calculated curve obtained from the kinetic modeling. All dα/dt curves presented in the following of this article are corrected.

The constantly decreasing reaction rate dα/dt, reported in Fig. 2, suggests that at least a diffusion step should be controlling the kinetic rate. Indeed, since the growth of ZnS proceeds outwards the initial ZnO particle (as further discussed in Section 3.3), the rate of the reaction should increase if the rate-determining step of growth was located on the outer surface, or remain constant if the rate-determining step of growth was located at the internal interface.

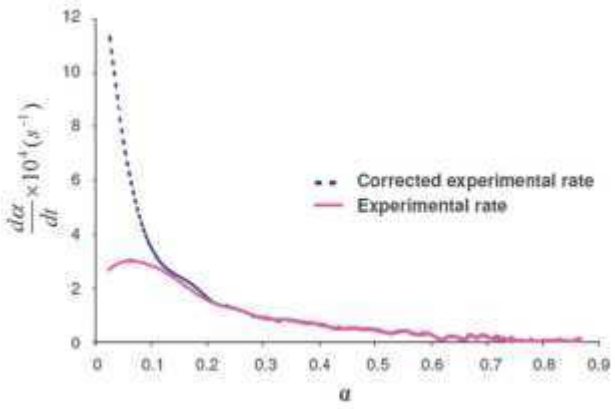

Figure 2 : Correction of the expérimental reaction rate of ZnO sulfidation at 310°C, $P(H_2S)$=5kPa and $P(H_2O)$=2,5kPa.

3.3. Materials characterizations

As shown in SEM micrographs reported in Fig. 3, ZnO material used in this study is made of monocrystalline ZnO rods exhibiting hexagonal sections. After sulfidation, at almost total conversion (α = 0.9), voids are observed inside the resulting ZnS particles, that have replaced the initial ZnO phase. The formation of voids at the ZnO–ZnS internal interface has also been evidenced by TEM observations for partially sulfided ZnO particles (Fig. 4). As reported more thoroughly in a previous paper,[26] these observations evidence a ZnS growth with an outward development during ZnO sulfidation, which may result from zinc and oxygen diffusion through the ZnS layer from the ZnO–ZnS internal interface to the ZnS surface.

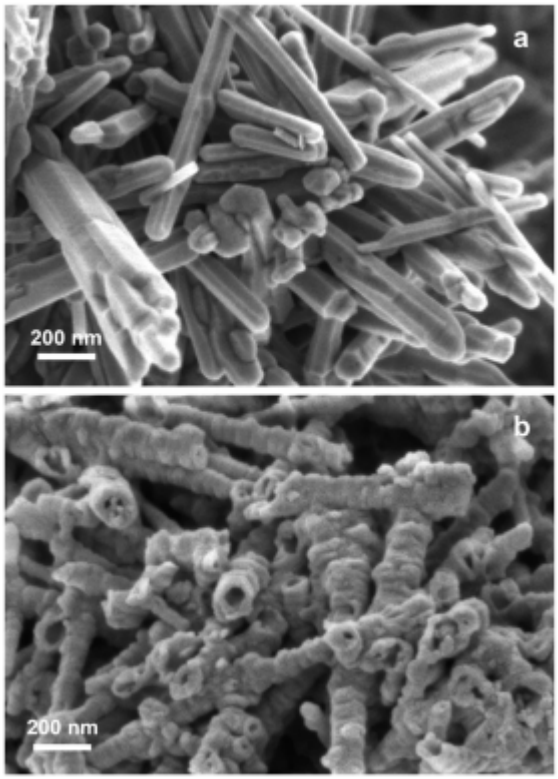

Figure 3: SEM micrographs of ZnO particles: (a) before sulfidation and (b) after sulfidation at 295°C and $P(H_2S)$=10 kPa (α=0.9)

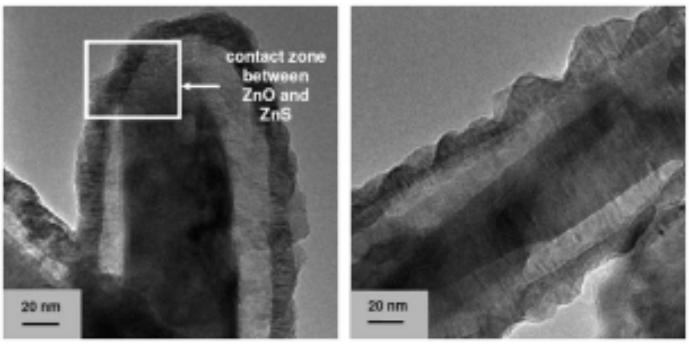

Figure 4: TEM micrographs of partially sulfided ZnO particles (α=0.3) at 230°C, $P(H_2S)$=5 kPa and $P(H_2O)$=2.5 kPa

Additional characterizations have been performed in order to get more information on the cavities formation during the ZnO sulfidation process. As conventional TEM analysis only provides a 2D-projection image of the sample, electron tomography[29–31] has been employed to study voids formation. Fig. 5 shows the TEM micrograph at 0° tilt angle of a partially sulfided ZnO particle. Fig. 6 shows some successive slices through the 3D volume obtained by electron tomography.

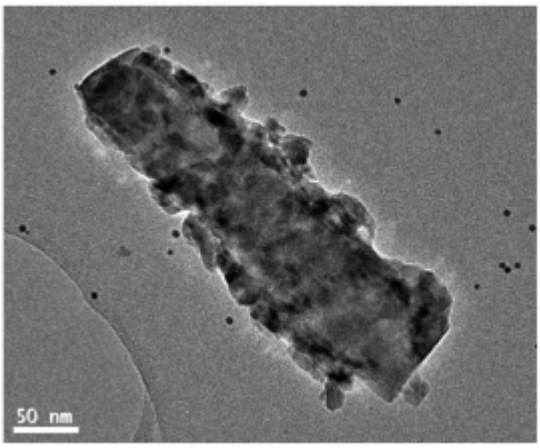

Figure 5 : TEM micrograph at 0°tilt angle of a partially sulfided ZnO particle (α=0.3) at 230°C, P(H_2S)=5 kPa and P(H_2O)=2.5 kPa. Gold nanoparticles (black dots) are used as fiducial markers for tilt series alignment.

The formation of a ZnS layer around the ZnO particle surface is clearly evidenced by electron tomography. Cavities are only observed on the ZnO surface (Fig. 6a for the upper ZnO surface, and Fig. 6f for the lower ZnO surface). Indeed, sections in the bulk of the ZnO particle do not show cavities (Fig. 6c and d6). Consequently, it seems that the voids formation only occurs at the ZnO–ZnS interface.

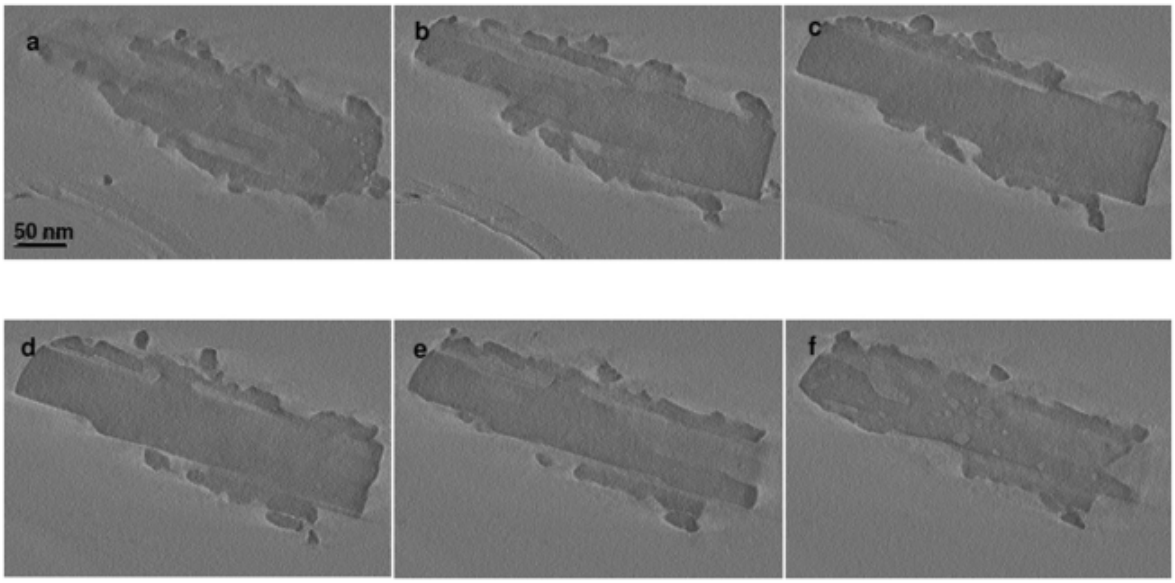

Figure 6 : Electron tomography study of a partially sulfided ZnO particle (α=0.3) at 230°C, P(H_2S)=5 kPa and P(H_2O)=2.5 kPa (from a to f). Numerical slices (0.55 nm thickness) of the 3D reconstruction in a perpendicular plane to the electron beam from the upper rod surface to the lower rod surface.

As an outward growth process of the ZnS phase is consistent with zinc and oxygen atoms diffusion through the ZnS layer toward the ZnS surface,[26] the nature of the point defects that may allow solid diffusion in the ZnS phase has been investigated. First investigations have been related to the study of the crystalline structure of the ZnS phase. Wurtzite is regarded in the literature as the sulfur deficient hexagonal ZnS phase, and sphalerite as the zinc deficient cubic ZnS phase.[32] XRD analysis performed on sulfided ZnO shows the formation of the mainly hexagonal ZnS phase (wurtzite). The comparison has been made to the literature values (JCPDS Pattern No. 04-008-7254) (cf. Fig. 8). However, the presence or absence of the cubic ZnS phase (sphalerite) cannot be clearly evidenced by XRD, as main sphalerite and wurtzite diffraction peaks at $2\theta \sim 28.6°$ might be overlaid. One may notice that relative intensities are not consistent with theoretical wurtzite XRD patterns calculated using Diamond software (3.1d version) for infinite crystal size (cf. Table 1). ZnS crystallites sizes have also been measured by XRD (Table 1), which shows that nanometric monocrystalline ZnS particles (~10 nm) were formed during sulfidation of ZnO samples at 310°C. Some ZnS particles were also measured by TEM and show nanometric sizes of 6, 7, 9 or 10 nm (cf. Fig. 7).

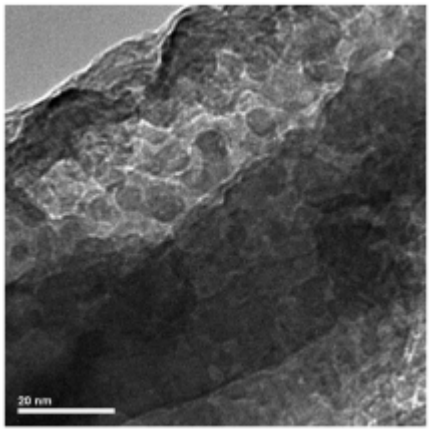

Figure 7: TEM micrograph of a partially sulfided ZnO particle (α=0.3) at 230°C, P(H_2S)=5 kPa and P(H_2O)=2.5 kPa.

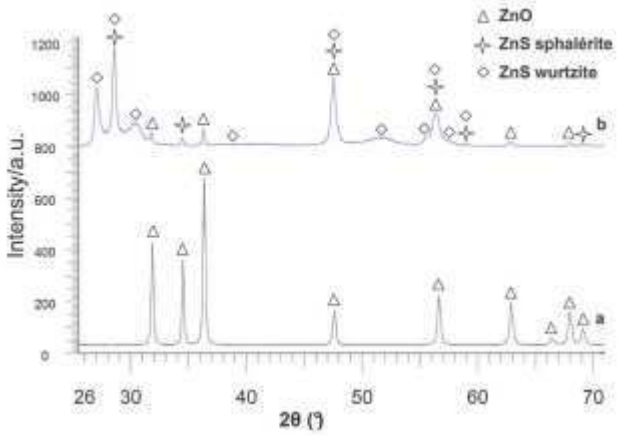

Figure 8 : XRD patterns obtained for (a) ZnO sample before sulfidation, (b) ZnO sample after sulfidation at 310°C, P(H_2S)=5 kPa and P(H_2O)=2.5 kPa (α=0.9).

Moreover, it is known that ZnS can form particles with a random stacking. It was shown that in this case the 102 peak of wurtzite (2θ = 39.6°) is absent and the 103 peak of wurtzite (2θ = 59°) is very broad.[33] However in the present experiments, the 102 peak of wurtzite (2θ = 39.6°) is absent but the 103 peak of wurtzite (2θ = 59°) is barely observed in Fig. 8 and is not broad. Therefore, a random stacking of the ZnS particles cannot be confirmed.

The structural study of the sulfided ZnO rods up to a fractional conversion a value of 0.9 has also been carried out by TEM and electron diffraction (in Selected-Area Electron Diffraction mode (SAED)) XRD study shows that the sulfided rod is composed of about 10 nm ZnS nanoparticles. However, the SAED pattern of a sulfided rod (Fig. 9) is formed of spots rather than rings, as expected for a polycrystalline material. It indicates that there exists an epitaxial relationship between the ZnS nanoparticles. Moreover, the most intense spots on the pattern (nonoriented) correspond to interplanar spacings, d values, characteristic to wurtzite: (100) at 3.31 Å and (110) at 1.91 Å. The ZnS particles orientation may consequently explain the deviation between the theoretical intensities of the wurtzite diffraction peaks on XRD patterns. Thus, very likely, ZnS sphalerite may not be present in the sulfided samples.

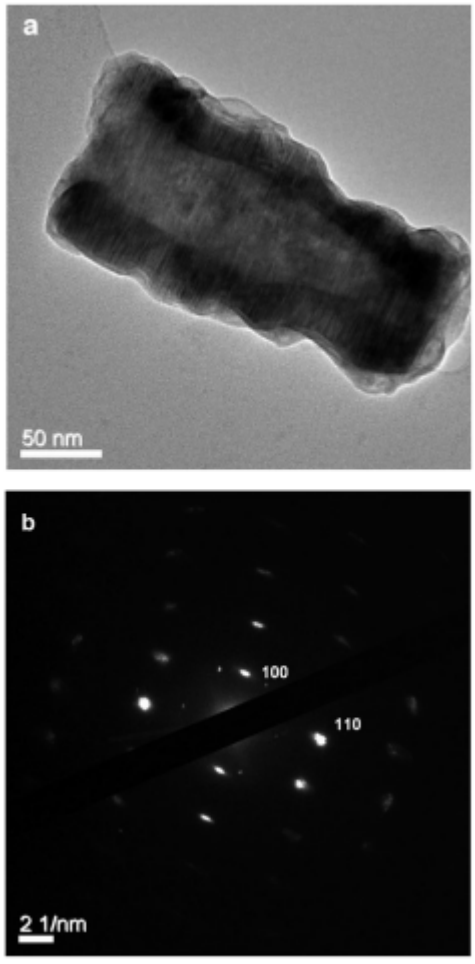

Figure 9 : (a) TEM micrograph of almost totally sulfided ZnO (α=0.9) at 295°C, P(H_2S)=5 kPa. (b) Selected-area electron diffraction pattern of the whole particle.

Some studies referring to sphalerite–wurtzite phase transformation and to point defects present in both ZnS crystalline phases can be found in the literature. Sphalerite and wurtzite are usually regarded as the low-temperature cubic and high-temperature hexagonal polymorphs, respectively.[35] However, more recently, it was shown that sphalerite–wurtzite inversion is not an invariant reaction at 1020°C at atmospheric pressure but depends on both sulfur pressure and temperature.[36] Indeed, when the H_2S pressure is high and the temperature is low, the sphalerite phase is formed preferentially. Luminescence studies have demonstrated that sulfur vacancies are produced in ZnS when it is heated in the vacuum or zinc vapor, and zinc vacancies when heated in sulfur vapor.[37] Some authors have examined phase changes in thin films consisting of a sphalerite and wurtzite mixture which were annealed in zinc and then in sulfur vapor between 850–1000°C. After heating in zinc vapor, the proportion of wurtzite was greatly increased. Annealing in sulfur vapor produced the reverse effect, the hexagonal phase changed to sphalerite.[38,39] Such observations suggest that sphalerite–wurtzite equilibrium conditions can be illustrated as shown in Fig. 10a.

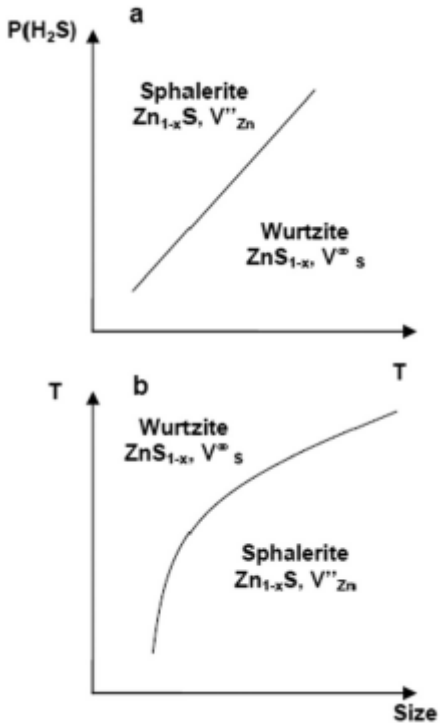

Figure 10 : Schematic representations of ZnS sphalerite–wurtzite phase transition, (a) [36–38] as a function of temperature and $P(H_2S)$, (b) [40] as a function of temperature and ZnS crystal size.

Considering the sulfidation experiments carried out for the present article, the ZnS sphalerite phase should be expected because of the low temperature (300°C) and the high H_2S partial pressure (>5 kPa). Moreover, the defects present in the ZnS phase resulting from the sulfidation reaction are more likely to be zinc vacancies, as sulfur vacancies are definitely not produced under sulfur vapor, and cationic point defects allow an external growth of the ZnS phase. Nevertheless, characterizations from both XRD and electron diffraction evidence wurtzite as the major phase after ZnO sulfidation. Several reasons may be argued to explain such a result:

-the nanometric size of ZnS particles: as it has been shown by several authors, the sphalerite to wurtzite transition temperature can be strongly reduced for low ZnS particles size (nanometric) as illustrated in Fig. 10b;[40–44]

-the formation of a possible solid solution Zn(S,O) due to substitution of sulfur sites by small amounts of oxygen. Because ZnO has the same structure as the wurtzite (hexagonal), the presence of oxygen in solid solution may play a role in promoting the formation of the hexagonal phase of ZnS.[45]

Therefore, the formation of the wurtzite hexagonal ZnS phase exhibiting zinc vacancies, allowing an external growth of ZnS, will be considered in the following. In order to study the reaction mechanism and to determine the rate-determining step, some kinetic assumptions have to be validated. These validations were carried out thanks to thermogravimetry experiments.

3.4. Rate-determining step assumption

In order to verify that the reaction kinetics is governed by a rate-determining step which remains the same over a large range of α values (0.2–0.8), we have used the method of jumps.[46] The existence of a rate-determining step can be shown by testing the validity of eqn (1), which states that the reaction rate is the product of two separable functions $\phi(T,P)$, depending on the operating conditions, and $S_m(t)$, depending on time. Thermogravimetric experiments were carried out to check this assumption, making successive jumps in temperature (or pressure) at different values of fractional conversion α. In Fig. 11, reaction rates $d\alpha/dt$ ratio values as measured just after and before a sudden change in temperature are plotted as a function of α. During a jump, the value taken by the S_m function should remain practically constant, whereas the value of the areic reactivity of growth, ϕ, should depend on the temperature. The ratio between the rate measured after the temperature change (v_a) and the rate measured before the change (v_b) should be equal to the ratio of $\phi(T_1)/\phi(T_0)$ according to eqn (4):

$$\frac{v_a(295°C)}{v_b(285°C)} = \frac{\frac{d\alpha}{dt}(T_1,t)}{\frac{d\alpha}{dt}(T_0,t)} = \frac{\phi(T_1)S_m(t)}{\phi(T_0)S_m(t)} = \frac{\phi(T_1)}{\phi(T_0)} \qquad (4)$$

where T_1 and T_0 are, respectively, the temperature after and before a sudden change. Each experimental point represented in Fig. 11 corresponds to a temperature jump of 10°C from 285°C to 295°C performed during an experiment started each time with a fresh ZnO sample. The rates after and before a jump were calculated by differentiating the curves representing the fractional conversion function of time on both sides of the jump.

The results reported in Fig. 11 show that the rate ratios remain approximately constant in the α range 0.2–0.8, so that it can be concluded that under these conditions eqn (1) and therefore the assumption of a rate-determining step are valid.

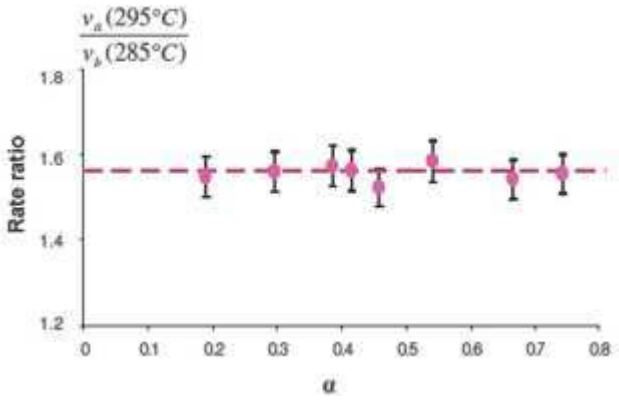

Figure 11 : Ratios of the rates after and before the jumps from 285 to 295°C as a function of α, P(H_2S)=5 kPa.

3.5. Instantaneous nucleation assumption

As previously recalled, the reaction between ZnO and H_2S involves nucleation and growth processes. In order to check whether during the reaction one of both processes can be considered as instantaneous compared to the other (otherwise nucleation and growth kinetics should lead to more complex models), a second type of experimental test can be performed.

In the limiting cases of instantaneous nucleation or growth the S_m function may be rewritten as a function of α. The kinetic rate can therefore be written as in eqn (5):

$$\frac{d\alpha}{dt} = \phi(T, P_i) S_m(\alpha) \quad (5)$$

An experimental test, as described by Pijolat et al.,[47] consists of performing two successive experiments under two distinct operating conditions Y_1 and Y_2 . At instant t = t_1, the operating conditions of the second experiment are suddenly changed from Y_1 to Y_2. It was shown that if the rate curves superimpose after instant t_1, then the reaction should proceed according to a limiting case. Here, two experiments were carried out under a fixed H_2S partial pressure equal to 5 kPa. The first experiment was achieved at 295°C. The second experiment was started at 285°C until a fractional conversion of 0.17 then the temperature was suddenly changed to 295°C, and the transformation was continued at 295°C until the end of the experiment. As shown in Fig. 12, the rate curves are superimposed after the temperature jump, which means that one of the growth or nucleation processes should be instantaneous toward the other processes. Therefore, the sulfidation reaction is a limiting case and the rate of the reaction can be written as in eqn (5). It also means that the sulfidation kinetics does not depend on the solid history before reaching the same temperature and pressure conditions.

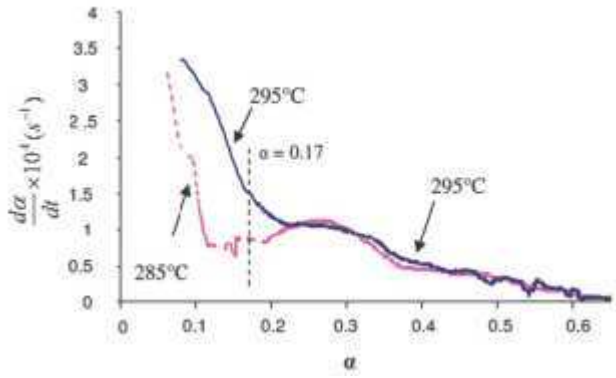

Figure 12 : Sudden temperature change from 285 to 295°C at α=0.17 and comparison to the experiment done at 295°C, P(H_2S)=5 kPa.

Moreover, electron micrograph observations of sulfided ZnO for very low fractional conversion (α ≈ 0.01) show that all ZnO particles are entirely covered with a thin layer of ZnS (Fig. 13). Indeed, a textural transformation is observed between ZnO before sulfidation and after sulfidation. Initial surfaces of ZnO rods are smooth (monocrystalline particles), whereas they become rough after some minutes of sulfidation at 295°C and 10 kPa (α ≈ 0.01) due to the formation of a thin layer of polycrystalline ZnS. Consequently, it can be concluded that the nucleation process is instantaneous toward the growth process.

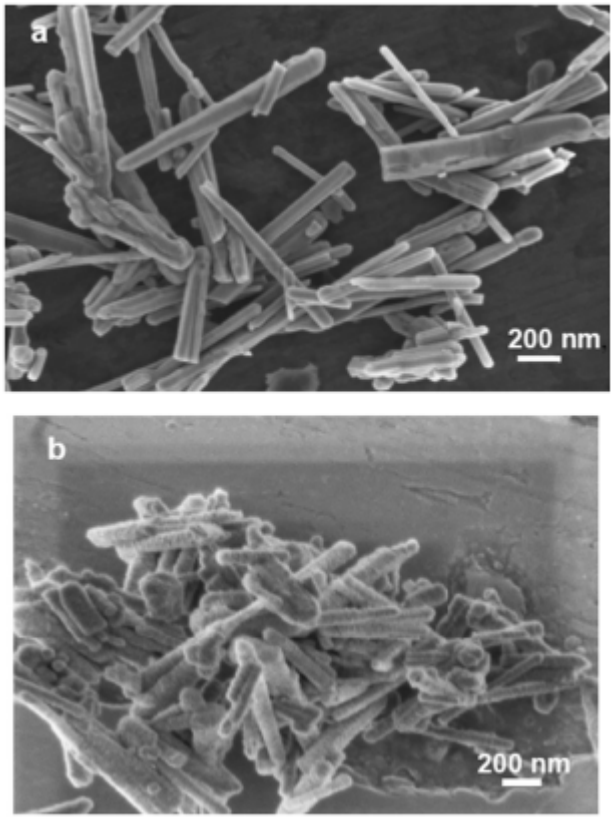

Figure 13 : SEM micrographs of ZnO particles: (a) before sulfidation and (b) after sulfidation at 295°C and P(H_2S)=10 kPa at very low fractional conversion (α≈0.01).

3.6. Influence of H2S partial pressure

An analysis of the influence of the H_2S and H_2O partial pressures on the reaction kinetics has been carried out thanks to the kinetic curves $d\alpha/dt$ as a function of fractional conversion α obtained with various pressure conditions. Since eqn (5) has been shown to well describe the kinetic rate, it is possible to plot the values of $d\alpha/dt$ measured at a given value of α (for example α = 0.2, and α = 0.3 in Fig. 14) as a function of $P(H_2S)$.

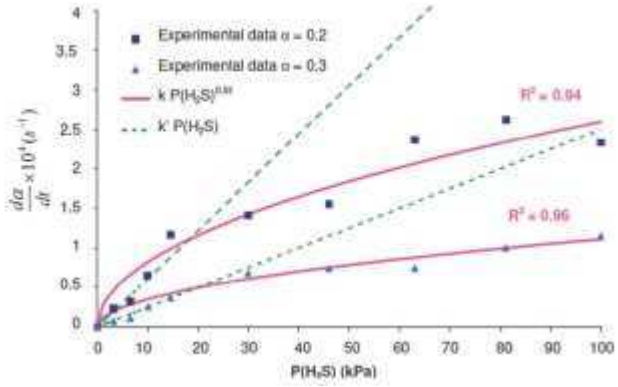

Figure 14 : Variation of the kinetic rate versus $P(H_2S)$ of ZnO sulfidation for the same fractional conversion (α=0.2 and α=0.3) at 260°C, $P(H_2S)$ variable up to 100 kPa, $P(H_2O)$=1.8 kPa.

The experimental values of reaction rate represented in Fig. 14 follow a law, which might vary according to the equation $v = kP(H_2S)^b$, with $b < 1$, while most studies report a linear variation of reaction rates toward H_2S partial pressures $P(H_2S)$.[11,20] This might be explained by the fact that much weaker $P(H_2S)$ and narrower partial pressure ranges were considered. Indeed, to our knowledge no data on the influence of H_2S partial pressure on ZnO sulfidation reaction for values higher than 4 kPa have been published. This might have led to an incorrect determination of the order of reaction with respect to $P(H_2S)$.

In order to confirm this result, additional thermogravimetry experiments were performed using the sudden change or jump method.[28] The dependence of the reaction rate, toward H_2S partial pressure, can also be studied by performing H_2S partial pressure jumps (for the same fractional conversion) up to various $P(H_2S)$ values. Observing the dependence of rate ratios versus H_2S partial pressure, $P(H_2S)_a/P(H_2S)_b$, allows us to follow the ϕ dependence toward H_2S partial pressure, as evidenced by eqn (6):

$$\frac{v_a\left(P(H_2S)_a\right)}{v_b\left(P(H_2S)_b\right)} = \frac{\phi\left(T, P(H_2S)_a\right)S_m(\alpha)}{\phi\left(T, P(H_2S)_b\right)S_m(\alpha)} = \frac{\phi\left(P(H_2S)_a\right)}{\phi\left(P(H_2S)_b\right)} \qquad (6)$$

During an experiment with $P(H_2S)_b$ condition, at a given fractional conversion the H_2S partial pressure is suddenly changed to another H_2S partial pressure, $P(H_2S)_a$. For a sulfidation with constant H_2S partial pressure ($P(H_2S)_b = (P(H_2S)_a$), the reaction ratio is equal to 1. Several jumps were carried out from the same H_2S partial pressure ($P(H_2S)_b$ = 1.4 kPa) to various H_2S partial pressures up to 100 kPa at a constant fractional conversion α = 0.34. By calculating the ratios between the rates measured just after and before a jump, the variation of f versus $P(H_2S)$ can be obtained as shown in Fig. 15.

It can be observed in Fig. 15 that the values of the kinetic rate ratios might follow, as well as previously in Fig. 11, the equation $v = kP(H_2S)^b$, with $b < 1$ better than a linear variation (higher regression coefficient). To conclude, the kinetic rate is not linear toward H_2S partial pressure but might vary according to the equation $v = kP(H_2S)^b$, with $b < 1$ on the H_2S partial pressure domain explored (3.3 kPa to 100 kPa).

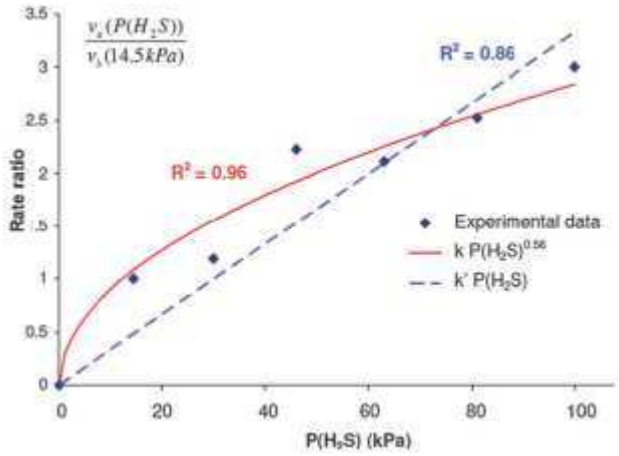

Figure 15 : Ratios of the kinetic rates after and before the jumps from a H_2S partial pressure of 14.5 kPa to various H_2S partial pressures as a function of $P(H_2S)$ at 260°C, $P(H_2O)$=1.8 kPa, α=0.34.

3.7. Influence of H_2O partial pressure

The variation of the kinetic rate toward H_2O partial pressure has been studied by thermogravimetry. Three isothermal ZnO sulfidation experiments were performed under the same H_2S partial pressure and various H_2O partial pressures $P(H_2O)$: without adding H_2O to the reacting gas ($P(H_2O) = 0$), with $P(H_2O)$ =1.25 kPa, and $P(H_2O)$ = 2.5 kPa. As shown in Fig. 16, resulting $\alpha(t)$ obtained are all identical. Consequently, H_2O partial pressure has no influence on the ZnO sulfidation reaction kinetics. Thus, the ϕ function does not depend on the H_2O partial pressure.

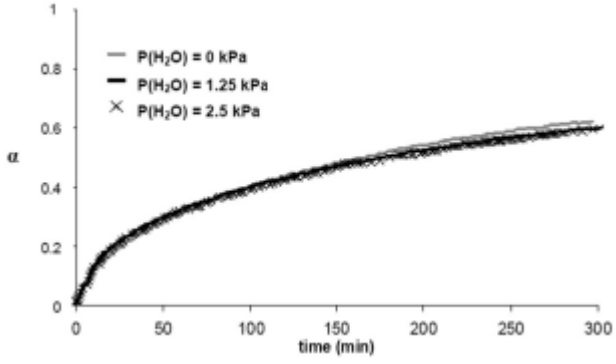

Figure 16 : Variation of the fractional conversion versus time of ZnO sulfidation at 295°C, $P(H_2S)$=5 kPa and various $P(H_2O)$.

4. ZnS phase growth mechanism

4.1. Proposition of elementary steps involved in the reaction

As previously discussed according to the materials characterizations, a mechanism of ZnS growth with outward development can be proposed. This implies zinc and oxygen diffusion from the ZnO–ZnS internal interface to the ZnS surface. The external development is made possible with the presence of zinc vacancies in the ZnS phase. Moreover, as explained in Section 3.3, the most probable point defects expected in the ZnS phase in the sulfidation operating conditions are zinc vacancies. Therefore, zinc ions should diffuse via zinc vacancies. Oxygen atoms may diffuse via interstitial sites. A mechanism can be proposed that considers the diffusion reactions through ZnO and ZnS crystals point defects (Kröger–Vink notation). The following eight steps are detailed in Table 2.

4.2. Determination of the rate-determining step

Assuming one of the eight steps (1) to (8) is the rate-determining step, eight possible rate laws corresponding to each of these eight steps can be calculated. For each possibility, a system of equations based on equilibrium conditions applied to the nonrate-determining steps, and on the electro-neutrality conditions has to be solved. Table 3 reports the possible expressions of the areic reactivity of growth for each of the elementary steps supposed to be rate-determining. These expressions are simplified considering the experimental conditions chosen for the study are far from the equilibrium conditions, otherwise the rate of the reverse reaction would have been taken into account. In the case of a diffusion rate-determining step (steps (4) and (5)), growth laws are expressed in terms of $\phi\ell_0$ instead of ϕ, ℓ_0 being a length equal to 1 m, in order to maintain units homogeneity (D represents diffusion coefficients).

The notation used are k_i ($1 \leq i \leq 8$) for the kinetic constants, K_i ($1 \leq i \leq 3$ and $5 \leq i \leq 8$) for the equilibrium constants, i corresponding to each of the steps and y for the sites fraction at the ZnS surface.

(1) H_2S dissociative adsorption at the ZnS surface

$H_2S + 2\ s + s' \rightarrow 2\ H\text{-}s + S\text{-}s'$

(2) External interface reaction with desorption of water at the ZnS surface

$2\ H\text{-}s + O''_{i\,ext} + 2\ h^{\circ}_{ext} \rightarrow H_2O + 2s$

(3) External interface reaction with creation of building units of ZnS at ZnS surface (sulfide ion and zinc vacancy)

$S\text{-}s \rightarrow S_{S\,ext} + s' + V''_{Zn\,ext} + 2\ h^{\circ}_{ext}$

(4) Zinc ion diffusion *via* zinc vacancies from the ZnO-ZnS internal interface to the surface of the ZnS layer

$V''_{Znext} \rightarrow V''_{Zn\,int}$

$Zn_{Znint} \rightarrow Zn_{Znext}$

(5) Oxygen diffusion through the ZnS layer from the internal interface to the ZnS surface *via* interstitial sites

$O''_{i\,int} \rightarrow O''_{int\,ext}$

(6) Internal interface reactions with creation of an oxygen vacancy in the ZnO phase and jump of an oxygen ion at an interstitial site of the ZnS phase

$O_{O(ZnO)} \rightarrow V^{\circ\circ}_{O(ZnO)} + O''_{i\,int}$

(7) Internal interface reaction with creation of a zinc vacancy in the ZnO phase

$Zn_{Zn(ZnO)} + V''_{Znint} \rightarrow Zn_{Zn\,int} + V''_{Zn(ZnO)}$

(8) Annihilation reaction between zinc and oxygen vacancies, which leads progressively to the formation of voids into the bulk of the ZnO phase

$V''_{Zn(ZnO)} + V^{\circ\circ}_{O(ZnO)} \rightarrow \emptyset$

Table 2 : Elementary steps proposed for the ZnO sulfidation mechanism, where s and s' represent free adsorption sites on the ZnS surface, the subscripts ext and int, respectively, refer to the external and internal interface, V''_{Zn} and $V^{\circ\circ}_{O}$ correspond, respectively, to a zinc and oxygen vacancy, O''_i to an oxygen atom located in an interstitial site, and Zn_{Zn} to a zinc atom located in a zinc position in the crystal structure.

It is interesting to compare these rate laws to the experimental results considering the kinetic rate dependence towards H_2S and H_2O partial pressures. The laws ϕ_5 and ϕ_6 do not depend on the gases partial pressures. Three laws (ϕ_4, ϕ_7 and ϕ_8) depend on the ratio $P(H_2S)/P(H_2O)$. The law ϕ_1 has a linear variation with $P(H_2S)$ but also a dependence toward $P(H_2O)$. Finally, only the ϕ_2 and ϕ_3 laws exhibit a nonlinear variation with $P(H_2S)$, but as these steps are located on the external interface, they would lead to an increasing reaction rate versus a since the surface of the particles continuously increases up to the end of the transformation (outward development). Consequently, none of the eight growth laws reported in Table 3 is consistent with a kinetic rate decreasing versus a, increasing versus $P(H_2S)$, and independent toward $P(H_2O)$. Therefore, a possible way to account for the experimental data was to combine two elementary steps assuming that both are controlling the kinetics. Such treatment, called ''mixed kinetics'', is based on the assumption that the kinetic rates of both steps are equal.

Rate limiting step	Φ law

(1) $$\phi_1 = k_1 P H_2 S \theta_s^{\,2} \theta_{s'} = k_1 P_{H_2S} \left(\frac{1}{1 + \frac{\sqrt{P_{H_2O}}}{2\sqrt{K_2} K_6^{\,3/2} K_8^{\,3/4}}} \right)^2 \left(\frac{1}{1 + \frac{4 K_6^{\,2} K_7 K_8^{\,3/2}}{K_3}} \right)$$

(2) $$\phi_2 = \theta_{H-s}^{\,2} [O''_{i\,ext}][h^{\circ}_{ext}] = k_2 \left(\frac{1}{1 + \frac{2 K_6 \sqrt{K_7} K_8^{\,3/4}}{\sqrt{K_1 K_3 P_{H_2S}}}} \right)^2 \times 4 K_6^{\,3} K_8^{\,3/2}$$

(3) $$\phi_3 = \theta_{S-s} = k_3 \left(\frac{1}{1 + \frac{P_{H_2O}}{K_1 K_2 \, 4 K_6^{\,3} K_8^{\,3/2} P_{H_2S}}} \right)$$

(4) $$\phi_4 l_0 = D|\Delta C| = D(V''_{Zn}) \quad \frac{K_1 K_2 K_3 K_6 \sqrt{K_8} P_{H_2S}}{P_{H_2O}}$$

(5) $$\phi_5 l_0 = D|\Delta C| = D(O''_i) \, K_6 \sqrt{K_8}$$

(6) $$\phi_6 = k_6$$

(7) $$\phi_7 = [V''_{Zn\,\mathrm{int}}] = k_7 \frac{K_1 K_2 K_3 K_6 \sqrt{K_8} P_{H_2S}}{P_{H_2O}}$$

(8) $$\phi_8 = [V''_{Zn(ZnO)}][V^{\circ\circ}_{O(ZnO)}] = k_8 \frac{K_1 K_2 K_3 K_6 K_7 P_{H_2S}}{P_{H_2O}}$$

Table 3 : Calculated possible ϕ growth laws in the approximations of the rate-determining steps for each step (1) to (8).

Oxygen diffusion (step (5)) and external interface reaction with water desorption (step (2)) have been considered leading to eqn (7) ($v_2 = v_5$):

$$k_2 \theta_{H-s}^2 [O''_{i,ext}][h^{\circ}_{ext}] S_{m2} = D_{O''_i} ([O''_{i,\mathrm{int}}] - [O''_{i,ext}]) S_{m5} \qquad (7)$$

The choice of mixed external interface reaction with water desorption and oxygen diffusion kinetics allows us to free oneself from the water partial pressure dependence. Thus, the rate

law of a mixed kinetics of external interface reaction with water desorption and oxygen diffusion has been calculated and is given by eqn (8):

$$v_{2,5} = \frac{aP_{H_2S}}{P_{H_2S} + b} \qquad (8)$$

with:

$$a = K_6 K_8^{1/2} D_{O_i^{"}} S_{m5} \quad ; \quad b = \frac{D_{O_i^{"}} S_{m5}}{k_2 K_1 K_3 K_7 K_8^{1/2} S_{m2}}$$

and where S_{m2} and S_{m5} functions, respectively, stand for the S_m function related to external interface reaction with water desorption and oxygen diffusion. These functions depend on the extent of the geometrical zone where the rate-determining step of growth occurs, which is the external interface for S_{m2} and the ZnS layer for S_{m5}. These functions can be calculated from geometrical considerations, as a function of particle shape.[27] For a cylinder the expressions are:

$$S_{m2} = \frac{2V_{mZnO}}{r_0}(1 + z\alpha)^{1/2} \qquad (9)$$

$$S_{m5} = \frac{4\ell_0 V_{mZnO}}{r_0^2 \ln(1 + z\alpha)} \qquad (10)$$

where V_{mZnO} represents the molar volume of ZnO (m^3 mol^{-1}), z the expansion coefficient ($V_{mZnS\ wurtzite}/V_{mZnO}$ = 1.66), r_0 the initial radius of the particle (m), ℓ_0 = 1 m. Thus the calculated rate varies with $P(H_2S)$ according to eqn (8), which can be compared to the experimental rate variation. Fig. 17 shows this comparison for the experimental data obtained at a fractional conversion of 0.3. Same results were obtained with other fractional conversions.

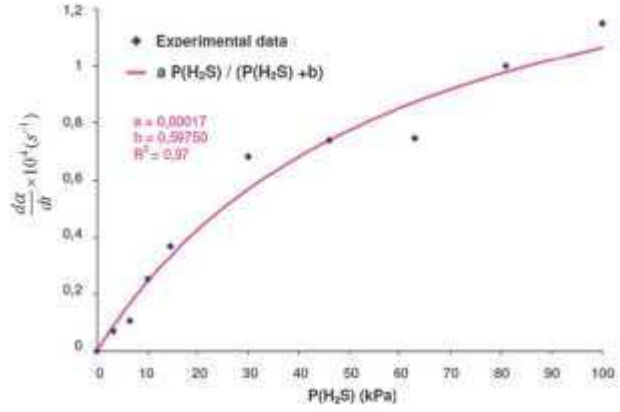

Figure 17 : Variation of the reaction rate versus $P(H_2S)$ of ZnO sulfidation for the same fractional conversion (α=0.3) at 260°C, $P(H_2S)$ variable up to 100 kPa, $P(H_2O)$=1.8 kPa.

The predicted variation is in good agreement with the experimental results. Therefore, the kinetic rate of the reaction is more likely to be controlled by a mixed kinetics of external interface reaction with water desorption and oxygen diffusion, as the rate variation exhibits a nonlinear dependence with $P(H_2S)$, which fits very well the experimental data, and no dependence with $P(H_2O)$ in agreement with experimental observations. It is worth noting that the vapor pressure has no influence on the reaction rate, while desorption of water molecules is one of the limiting steps. It can be explained by the fact that, far from the equilibrium, the desorption rate depends on intermediates which formation does not require water vapor pressure.

A mixed kinetics of zinc diffusion and external interface reaction with water desorption has also been considered, but the corresponding variation toward H_2S partial pressure was not in good agreement with the experimental data. A kinetic model can now be proposed in order to explain the variation of the experimental rate versus α.

4.3. Expression of the reaction rate

From eqn (8), (9) and (10), the expression of the reaction rate can be rewritten as in eqn (11):

$$v_{2,5} = \frac{k_2 K_1 K_3 K_6 K_7 K_8^{1/2} P_{H_2S} D_{0_i^{"}} S_{m2} S_{m5}}{k_2 K_1 K_3 K_7 K_8^{1/2} P_{H_2S} S_{m2} + D_{0_i^{"}} S_{m5}} \qquad (11)$$

However, according to microscopy observations, there is formation of voids at the internal interface which leads to a decrease in the contact area between ZnO and ZnS phases, which consequently slows down the kinetic rate. Therefore it is necessary to account for this phenomena by correcting the S_{m5} function with a surface fraction $F_c(\alpha)$ defined as in Eqn (12):

$$F_c(\alpha) = \frac{S_c(\alpha)}{S_0} \qquad (12)$$

where $S_c(\alpha)$ represents the contact surface between ZnO and ZnS phases at the internal interface at a given fractional conversion α, and S_0 the initial ZnO particle surface area. The variation of the surface fraction $F_c(\alpha)$ can be determined thanks to the modeling of nucleation and growth of voids at the internal interface in analogy with the Mampel model.[48] Since there is no analytical expression of $F_c(\alpha)$ for the considered geometry, this function has been obtained by means of numerical Monte Carlo calculations performed at different fractional conversions. The extension of this methodology to other particle geometries will be a subject of future work. The reaction rate can therefore be written according to eqn (13) by taking into account the decrease in the ZnO–ZnS interface:

$$v_{2,5} = \frac{k_2 K_1 K_3 K_6 K_7 K_8^{1/2} P_{H_2S} D_{0_i^{"}} S_{m2} F_c(\alpha) S_{m5}}{k_2 K_1 K_3 K_7 K_8^{1/2} P_{H_2S} S_{m2} + D_{0_i^{"}} F_c(\alpha) S_{m5}} \qquad (13)$$

It is worth noticing that single diffusion (step 5) and external interface reaction (step 2) rate determining steps are both included as limit cases in eqn (11). Moreover the expression of the reaction rate law can also be calculated by the law of additive reaction times involving oxygen

diffusion and external interface reaction with water desorption.[49] This law allows us to find the same expression as the one proposed. However, the use of this law is allowed only if some conditions are respected. Indeed, it must be a pseudo-steady state reaction, the two steps considered should belong to a linear mechanism and the multiplying coefficient of the linear combination, which allows us to obtain the global reaction, must be the same for both steps. In this case, these conditions are all fulfilled, that is why both calculations lead to the same rate expression.

It can be noticed that the fS m assumption (eqn (1)) should not be valid because of the presence of S_m functions in the denominator. Nevertheless kinetic tests showing that the ϕS_m assumption was verified can also be explained by some calculations. The rate law can be expressed as in eqn (14):

$$v_{2,5} = \frac{cS_{m2}S_{m5}}{S_{m2} + dS_{m5}} \qquad (14)$$

with:

$$c = \frac{F_c(\alpha)K_6 D_{O_i^{"}}}{k_2 K_1 K_3 K_7 P_{H_2S}} \quad ; \qquad d = \frac{F_c(\alpha)D_{O_i^{"}}}{k_2 K_1 K_3 K_7 K_8^{1/2} P_{H_2S}}$$

Indeed, the c and d values functions of temperature, as expressed in the rate law detailed in eqn (14), were obtained thanks to sulfidation experiments performed at four distinct temperatures. Fig. 18, which shows the variation of Ln(c) and Ln(d) versus 1/T, indicates an Arrhenius dependence with the temperature. Thus, c and d values may be evaluated for any temperature and the ratios of the rates before and after a temperature jump can be calculated using eqn (15):

$$\frac{v_{2,5\ d}(295°C)}{v_{2,5\ g}(285°C)} = \frac{\dfrac{c(295°C)S_{m2}S_{m5}}{S_{m2} + d(295°C)S_{m5}}}{\dfrac{c(285°C)S_{m2}S_{m5}}{S_{m2} + d(285°C)S_{m5}}} \qquad (15)$$

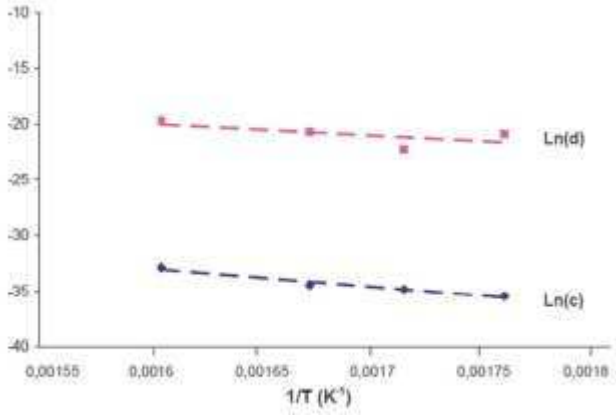

Figure 18 : Representation of Ln(c) and Ln(d) functions of 1/T for ZnO sulfidation reaction at various temperatures 295–310–325–350°C, P(H_2S)=5 kPa, P(H_2O)=2.5 kPa, where c and d are the values expressed in eqn (14).

Fig. 19 shows the calculated values of these ratios for a temperature jump from 285°C to 295°C at various fractional conversions.

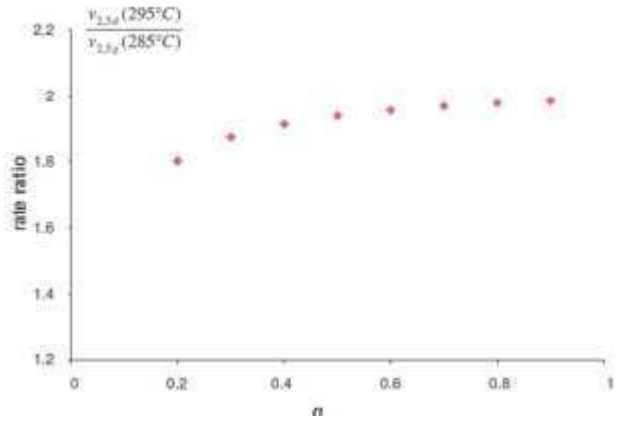

Figure 19 : Calculated rate ratios after and before the jumps from 285 to 295°C functions of α, P(H_2S)=5 kPa, P(H_2O)=2.5 kPa.

The calculated rate ratios do not vary significantly with the fractional conversion. This result might explain why the test validating the ϕS_m assumption was verified experimentally. Indeed, because of the measurement error and the weak variation of the calculated rate ratios, the experimental values remain approximately constant in the explored domain (from 0.2 to 0.8). Finally, the experimental rate of the sulfidation reaction can be confronted to the expression of the calculated rate assuming a constant ZnO–ZnS internal interface (eqn (11)) and the calculated rate taking $F_c(\alpha)$ into account (eqn (13)). An example of numerical fitting is presented in Fig. 20.

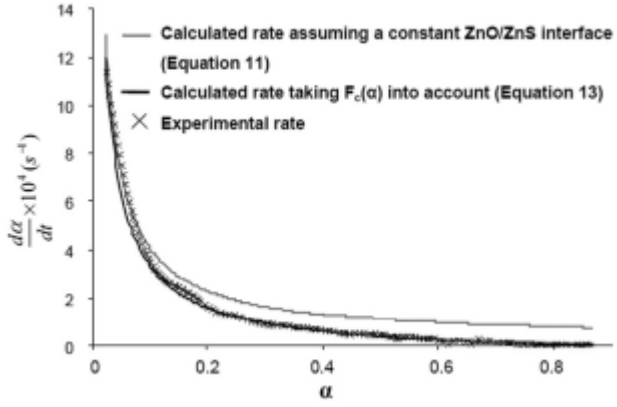

Figure 20 : Comparison between experimental and calculated reaction rates for ZnO sulfidation at 310°C, P(H_2S)=5 kPa and P(H_2O)=2.5 kPa. The calculated rates were determined assuming a constant ZnO–ZnS internal interface (grey line) and by taking $F_c(\alpha)$ into account (black line).

As shown in Fig. 20, calculated and experimental curves appear to be in rather good agreement but there is a slight deviation from a fractional conversion of 0.2. The gap observed between the experimental and the calculated curves can be explained by the formation of voids at the ZnO–ZnS internal interface, as shown by TEM and electron tomography characterizations (Section 3.3). The formation of these voids may lead to a decrease in the ZnO and ZnS phases contact area, and consequently this may strongly restraint the kinetic rate. When considering this phenomenon in the

kinetic modeling (eqn (13)), through the function $F_c(\alpha)$ (described in eqn (12)), very good agreement is observed between both experimental and calculated kinetic rates.

The same plot is presented in Fig. 21 under the form of fractional conversion a versus time. The calculated fractional conversions were obtained by numerical integration of the respective calculated (considering and not considering ZnO–ZnS interface surface fraction $F_c(\alpha)$) and experimental rates. Since the experimental data do not exceed a fractional conversion of 0.865, the integration was consequently stopped after reaching this value for both calculated curves. Fig. 21 shows the comparison between experimental and calculated fractional conversions.

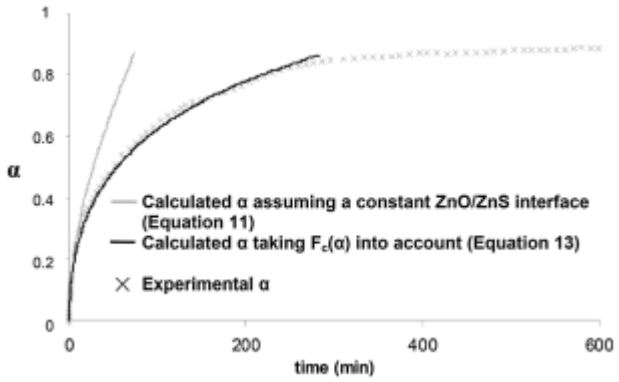

Figure 21 : Comparison between the experimental and calculated fractional conversions (from eqn (11) and (13)) for ZnO sulfidation at 310°C, $P(H_2S)$=5 kPa and $P(H_2O)$=2.5 kPa.

As expected, the calculated fractional conversion assuming a constant ZnO–ZnS interface is not in good agreement with the experimental data. On the other hand, the calculated fractional conversion obtained when taking $F_c(\alpha)$ into account is in much better agreement with the experimental data up to a fractional conversion of around 0.82. After this value, a discrepancy from the experimental curve is observed. This is due to the fact that the Mampel model fails to describe the strong experimental decrease in $F_c(\alpha)$ observed at high fractional conversion values (a > 0.6) as observed in Fig. 22. This phenomenon can be explained by the fact that Mampel modeling implies an isotropic growth while in our experiments the growth of cavities seems to be anisotropic (the growth rate appears to be more rapid along the ZnO–ZnS interface than along the radial direction). The regular void layer observed in Fig. 4 provides evidence for the anisotropic growth of cavities during ZnO sulfidation reaction.

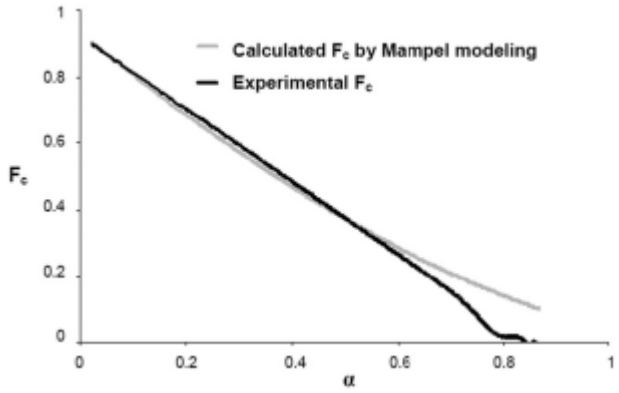

Figure 22 : Evolution of the calculated ZnO–ZnS interface surface fraction $F_c(\alpha)$ obtained by Mampel modeling and the experimental surface fraction $F_c(\alpha)$ obtained from the experimental and calculated rate curves for ZnO sulfidation at 310°C, $P(H_2S)$=5 kPa and $P(H_2O)$=2.5 kPa.

5. Conclusions

The kinetics of ZnO sulfidation by H2S has been investigated using isothermal and isobaric thermogravimetry. Characterizations have shown mainly the formation of the ZnS hexagonal phase composed of oriented nanoparticles. Eight elementary steps of the sulfidation reaction were proposed with the outward growth of ZnS and diffusion of zinc, via zinc vacancies, and oxygen, via interstitial sites, through the ZnS layer from the internal interface to the surface. Thermogravimetry experiments showing the influence of hydrogen sulfide and water partial pressures on the reaction kinetics have allowed us to determine the rate-determining step of the reaction. It was shown that water vapor has no influence on the reaction rate, whereas the reaction rate has a nonlinear variation with H2S partial pressure. A mixed kinetics of oxygen diffusion and external interface reaction with water desorption is more likely to control kinetically the reaction. Void formation at the internal interface leads to a decrease in the ZnO–ZnS internal interface and to a strong slowing down of the reaction rate. Consequently, this phenomenon has been taken into account in the kinetic modeling by balancing the S_{m5} function with a surface fraction $F_c(\alpha)$ accounting for the evolution of the contact area between the ZnO and ZnS phases during the reaction. The void formation has been represented by a random nucleation followed by an isotropic growth of cavities in analogy with the Mampel model.

An expression of the reaction rate, including the $F_c(\alpha)$ function, depending on the operating conditions, geometry of the particle and fractional conversion has been obtained. Very good agreement has been achieved between both experimental and calculated rates when taking into account the decrease in the ZnO–ZnS interface. Moreover, the same results were also obtained for other ZnO materials with different characteristics (size and shape). Finally, this study should contribute to a fundamental knowledge of the reaction that is, at the present time, missing in the literature.

Acknowledgements

The authors thank Florent Moreau and Anne-Lise Taleb (IFPEN) for their help performing SEM and TEM observations, electron diffraction and electron tomography. The authors also thank Michel Soustelle, Eric Serris and Ve´ronique Peres from the Ecole des Mines de Saint-Etienne for numerous and fruitful discussions. Finally, the authors thank Jean-Pierre Reyt (IFPEN) for technical help on thermogravimetry.

Notes and references

1 C. V. d. B. M. Higman, Gasification, Elsevier, 2003.
2 C. Ratnasamy and J. P. Wagner, Catal. Rev.: Sci. Eng., 2009, 51(3), 325–440.
3 A. Kohl and R. Nielsen, Gas purification, Gulf Publishing ed.,1997.
4 H. Schulz, Appl. Catal., A, 1999, 186(1–2), 3–12.
5 G. P. Van der Laan and A. A. C. M. Beenackers, Catal. Rev.:Sci. Eng., 1999, 41(3–4), 255–318.
6 W. Torres, S. S. Pansare and J. G. Goodwin, Catal. Rev.: Sci.Eng., 2007, 49(4), 407–456.
7 S. S. Pansare and J. D. Allison, Appl. Catal., A, 2010, 387(1–2),224–230.
8 A. Samokhvalov and B. J. Tatarchuk, Phys. Chem. Chem.Phys., 2011, 13, 3197–3209.
9 E. A. Efthimiadis and S. V. Sotirchos, Chem. Eng. Sci., 1993,48(11), 1971–1984.
10 M. C. Woods, S. K. Gangwal, K. Jothimurugesan and D. P. Harrison, Ind. Eng. Chem. Res., 1990, 29(7), 1160–1167.
11 E. A. Efthimiadis and S. V. Sotirchos, Chem. Eng. Sci., 1993,48(5), 829–843.
12 F. Huiling, L. Yanxu, L. Chunhu, G. Hanxian and X. Kechang, Fuel, 2002, 81(1), 91–96.
13 J. Szekely, J. W. Evans and H. Y. Sohn, Gas-solid reactions, Academic press ed., Londres, 1976.
14 J. B. Gibson and D. P. Harrison, Ind. Eng. Chem. Proc. Des. Dev., 1980, 19(2), 231–237.
15 P. V. Ranade and D. P. Harrison, Chem. Eng. Sci., 1981, 36, 1079–1089.
16 J. M. Davidson and K. Sohail, Ind. Eng. Chem. Res., 1995, 34(11), 3675–3677.
17 M. C. Woods, S. K. Gangwal, K. Jothimurugesan and D. P. Harrison, Ind. Eng. Chem. Res., 1990, 29(7), 1160–1167.
18 E. R. Monazam, L. J. Shadle and D. A. Berry, Chem. Eng. Sci., 2008, 63(10), 2614–2623.
19 I. I. Novochinskii, C. Song, X. Ma, X. Liu, L. Shore, J. Lampert and R. J. Farrauto, Energy Fuels, 2004, 18(2), 576–583.
20 Y. X. Li, H. X. Guo, C. H. Li and S. B. Zhang, Ind. Eng. Chem. Res., 1997, 36(9), 3982–3987.
21 H. Y. Yang, R. Sothen, D. R. Cahela and B. J. Tatarchuk, Ind. Eng. Chem. Res., 2008, 47(24), 10064–10070.
22 E. Sasaoka, S. Hirano, S. Kasaoka and Y. Sakata, Energy Fuels, 1994, 8(5), 1100–1105.
23 J. M. Davidson, C. H. Lawrie and K. Sohail, Ind. Eng. Chem. Res., 1995, 34(9), 2981–2989.
24 J. M. Davidson, J. D. Denny and C. H. Lawrie, J. Chem. Soc., 1989, 1695–1696.
25 S. Lew, A. F. Sarofim and M. Flytzani-Stephanopoulos, Ind. Eng. Chem. Res., 1992, 31(8), 1890–1899.

26 L. Neveux, D. Chiche, D. Bazer-Bachi, L. Favergeon and M. Pijolat, Chem. Eng. J., 2012, 181–182, 508–515.
27 M. Soustelle, Handbook of heterogeneous kinetics, Wiley, 2010.
28 M. Soustelle and M. Pijolat, Solid State Ionics, 1997, 95(1–2), 33–40.
29 O. Ersen, C. Hirlimann, M. Drillon, J. Werckmann, F. Tihay, C. Pham-Huu, C. Crucifix and P. Schultz, Solid State Sci., 2007, 9(12), 1088–1098.
30 A. H. Janssen, A. J. Koster and K. P. de Jong, Angew. Chem., Int. Ed., 2001, 40(6), 1102–1104.
31 M. Weyland, P. A. Midgley and J. M. Thomas, J. Phys. Chem. B, 2001, 105(33), 7882–7886.
32 D. J. Vaughan, Sulfide mineralogy and geochemistry, 61st edn, 2006.
33 H. Z. Zhang and J. F. Banfield, J. Phys. Chem. C, 2009, 113(22), 9681–9687.
34 J. I. Langford and A. J. C. Wilson, J. Appl. Crystallogr., 1978, 11(2), 102–113.
35 E. T. Allen and J. L. Crenshaw, Am. J. Sci., 1912, 34(4), 341–396.
36 S. D. Scott and H. L. Barnes, Geochim. Cosmochim. Acta, 1972, 36(11), 1275–1295.
37 F. A. Kro¨ger and H. J. Vink, Physica, 1954, 20(7–12), 950–964.
38 N. K. Morozova, M. M. Veselkova, A. F. Botnev and K. V. Shalimova, Crystallogr. Rep., 1969, 14, 74–78.
39 T. Bansagi, E. A. Secco, O. K. Srivastava and R. R. Martin, Can. J. Chem., 1968, 46(18), 2881–2886.
40 H. Z. Zhang, F. Huang, B. Gilbert and J. F. Banfield, J. Phys. Chem. B, 2003, 107(47), 13051–13060.
41 M. B. Geilikman, Phys. Chem. Miner., 1982, 8(1), 2–7.
42 F. Huang and J. F. Banfield, J. Am. Chem. Soc., 2005, 127(12), 4523–4529.
43 S. Li, J. S. Lian and Q. Jiang, Chem. Phys. Lett., 2008, 455(4–6), 202–206.
44 S. B. Qadri, E. F. Skelton, D. Hsu, A. D. Dinsmore, J. Yang, H. F. Gray and B. R. Ratna, Phys. Rev. B: Condens. Matter Mater. Phys., 1999, 60(13), 9191–9193.
45 B. J. Skinner and P. B. Barton, Jr., Am. Mineral., 1960, 45, 612–625.
46 M. Pijolat and M. Soustelle, Thermochim. Acta, 2008, 478(1–2), 34–40.
47 M. Pijolat, F. Valdivieso and M. Soustelle, Thermochim. Acta, 2005, 439(1–2), 86–93.
48 K. L. Mampel, Z. Phys. Chem., Abt. A, 1940, 187, 235–249.
49 H. Y. Sohn, Metall. Trans. B, 1978, 9(1), 89–96. Paper